Journal Pre-proof

Influence of UV irradiation on mechanical properties and drop-weight impact performance of polypropylene biocomposites reinforced with short flax and pine fibers

Khaled Nasri Ph.D. student , Lotfi Toubal Professor ,
Éric Loranger Professor , Demagna Koffi Professor

PII: S2666-6820(22)00060-3
DOI: https://doi.org/10.1016/j.jcomc.2022.100296
Reference: JCOMC 100296

To appear in: *Composites Part C: Open Access*

Received date: 30 May 2022
Revised date: 4 July 2022
Accepted date: 11 July 2022

Please cite this article as: Khaled Nasri Ph.D. student , Lotfi Toubal Professor , Éric Loranger Professor , Demagna Koffi Professor , Influence of UV irradiation on mechanical properties and drop-weight impact performance of polypropylene biocomposites reinforced with short flax and pine fibers, *Composites Part C: Open Access* (2022), doi: https://doi.org/10.1016/j.jcomc.2022.100296

Influence of UV irradiation on mechanical properties and drop-weight impact performance of polypropylene biocomposites reinforced with short flax and pine fibers

Khaled Nasri[1], Lotfi Toubal[1]*, Éric Loranger[1], Demagna Koffi[1]

[1]Mechanical engineering department, Innovations Institute in Ecomaterials, Ecoproducts and Ecoenergy (I2E3), Université du Quebec à Trois-Rivières (UQTR), C.P. 500 Trois-Rivières (Quebec), G9A 5H7 Canada

Ph.D. student: khaled.nasri@uqtr.ca; Professor: lotfi.toubal@uqtr.ca, Tel. +18193765011#3970; Professor: Eric.Loranger1@uqtr.ca, Tel. +18193765011#4518 ; Professor: Demagna.koffi@uqtr.ca, Tel. +18193765011#3910

Highlights:

- We evaluated the mechanical performances of flax and pine short-fiber-reinforced polypropylene biocomposite.
- The influences of natural fibers, irrespective of the lignin content, on the mechanical properties and impact behavior of ultraviolet (UV)-altered short natural fiber-reinforced thermoplastic is investigated.
- Damage are detected by using acoustic emission, and X-ray Micro-computed tomography.
- High lignin biocomposite bares less property degradation after accelerated UV irradiation.
- UV irradiation and damage mechanisms are highly material dependent.

Abstract

The design of biocomposite structures for outdoor applications should consider the influence of ultraviolet (UV) irradiation on the mechanical performances to more accurately determine their durability characteristics and prevent significant damage. Ultraviolet radiation causes the discoloration, surface roughness, mass loss, and degradation of the mechanical properties of biocomposites. In this study, the flexural strength and low-velocity impact response of polypropylene reinforced with short flax or pine fibers, which differed with respect to their physical and chemical properties, were investigated. Flax fibers are twice the length of pine

fibers, and exhibit higher cellulose contents. Moreover, flax fibers have been demonstrated to increase the flexural strength and impact resistance of biocomposites. However, under UV irradiation, pine fibers containing more lignin dampened the degradation. Under photo-oxidative conditions, lignin is degraded to protect crystalline cellulose by acting as a light-absorbing compound. Non-destructive techniques such as Fourier transform infrared spectroscopy (FTIR), colorimetry, confocal imaging, acoustic emission, and CT scanning were therefore used to evaluate the effect of UV radiation on the chemical properties, color change, surface roughness, bending behavior, and drop-impact damage.

Keywords: Biocomposites, UV irradiation, Residual properties, Low-velocity Impact, flax and pine fibers; failure analysis, Non-destructive analysis.

1. Introduction

Biocomposites, particularly short natural fiber-reinforced thermoplastic (SNFT) composites, have recently attracted significant industrial interest, and are typically used in the automotive industry, packaging, and construction sector [1,2]. The advantages of biocomposites include the cost and properties such as low density, excellent mechanical properties, and environmental friendliness [1,3]. However, it should be noted that these biocomposites allow for the manufacture of parts with complex shapes (gears, etc.) in a single injection molded element. However, the sensitivity of natural fibers to the climatic environment limits the use of biocomposites in exterior applications, as previously reported [4–16].

Several researchers studied the durability of biocomposites by considering the variations in climatic conditions in several regions of the world, namely the tropical, Mediterranean, and continental regions [17–20]. Biocomposites degrade under the effects of a combination of environmental factors such as temperature, humidity, ultraviolet (UV) rays, and biological attack. In previous studies, laboratory UV-weathering chambers were used to accelerate the degradation process and predict the alteration of materials [6,7,16,21]. The advantage of accelerated aging tests is related to their capacity to reproduce (within several weeks) the degradation of biocomposites, which generally occurs outdoors over months or years. In addition, using accelerated aging testers, the contribution of each factor (humidity, UV, etc.) to degradation can be quantified. In particular, high temperatures and UV irradiation generate photo-oxidation in biocomposites; thus causing discoloration, increased surface roughness,

mass loss, and a degradation of the mechanical properties such as the tensile strength and Young's modulus. Extensive reviews of the literature on biocomposite aging have been provided in [22,23].

The decrease in the SNFT performance under the effect of inclement weather is largely due to the degradation of natural fibers [24]. However, the degradation of natural fibers is dependent on their chemical and physical characteristics [25]. Peng et al. 2015 [16] studied the influence of the chemical composition of natural fibers (cellulose, hemicellulose, and lignin) on the accelerated deterioration of polypropylene SNFT reinforced with short wood fibers. It was reported that the removal of lignin from natural fibers results in a relatively higher stiffness and mechanical strength. However, under UV irradiation, cellulose promoted the formation of microcracks on the surface of the biocomposite samples, thus promoting the degradation of the mechanical properties. This indicates that lignin can act as a degradation inhibitor. Similarly, Beg K. L. (2008) [6] studied the accelerated weathering of bleached and unbleached PP /Kraft biocomposites. Bleached Kraft fiber biocomposites (%lignin < 1%) exhibited increased degradation in terms of the mechanical strength and impact resistance due to the absence of lignin in the fiber structure. Moreover, Stark et al 2006 [26] reported that injection-molded Polypropylene/50% short wood fibers biocomposites are more resistant to UV irradiation than thermocompression-molded samples, as they exhibit a more significant encapsulation of fibers by a matrix layer. In a more recent study, Ratanawilai and Taneerat (2018) [27] found that SNFT based on PP demonstrated an improved weather resistance than SNFT based on low-density polyethylene (LDPE), high-density polyethylene (HDPE), and polyvinyl chloride (PVC).

In the abovementioned studies, the influence of natural fiber and its chemical and physical structures on the aging of SNFT was determined; and in most of these studies, the degradation of mechanical properties was evaluated primarily based on quasi-static tests (traction and/or bending), in addition to Izod tests. However, SNFT structures designed for exterior applications are vulnerable to low-speed impact. Significantly few studies were conducted on the low-speed impact of SNFT [28,29]. As mentioned previously, the impact on SNFT at impact causes damages (cracks and indentations), which are proportional to the impact speed. Moreover, as reported, this damage can be attributed to different fiber/matrix interactions; and therefore, to the SNFT damage mechanisms. However, with reference to the literature, few studies considered the influence of UV irradiation on the drop-weight impact performance of short

natural fiber-reinforced thermoplastic composites; and in particular, the influence of lignin and its role in stabilizing the impact performance after the UV irradiation of SNFT [30].

The aim of this study was to determine and evaluate the influence of natural fibers, Whether rich or poor of the lignin content, on the mechanical properties and the impact behavior of UV-altered SNFT. Hence, an injected polypropylene reinforced with 30% flax fibers or pine wood fibers was evaluated in this study. The visual aspect (color and roughness), chemical properties, and mechanical properties were monitored throughout the alteration. The mechanical behavior was assessed based on quasi-static bending and low-speed impact tests. Using an acoustic emission (AE) technique, the damage was monitored in real-time during the bending tests. The evolution of cracks during bending tests were monitored using a charge-coupled device (CCD) camera, and the damage induced by the drop-weight impact test was observed using three-dimensional (3D) X-ray tomography.

2. Materials and Methods

2.1. Samples and manufacturing method

The biocomposite grains PP30-F (polypropylene reinforced with 30% by the weight of flax fiber "FF30P233-00") and PP/30P (polypropylene reinforced with 30% by the weight of the pine fiber "WP30P233-00") purchased from Rhetech, USA, were used in this study. Natural fibers mainly consist of cellulose, hemicellulose, and lignin. With reference to the literature, Table 1 presents the chemical composition of natural fibers and their géometrical, physical and mechanical properties. Based on the data, it was found that pine fibers are rich in lignin, and flax fibers low in lignin exhibit significantly high cellulose and hemicellulose contents.

In accordance with the ASTM D-790 and ASTM D-2856 standards, the bending and impact samples were injection-molded at a temperature of 200 °C using an AlorAir Zeus ZTR 900 press with a capacity of 100 t (Zhafir plastic machines distributed by Haitien; Zeres Series; ZE900/210). Prior to injection, the granules were dried in an oven at a temperature equivalent to T = 80 °C for 2 h, to eliminate the humidity in the fibers, and therefore reduce or prevent microvoids in the samples after injection.

***Table 1**. Chemical, geometrical, physical, and mechanical properties of natural fibers.*

Materials	Chemical properties*	Géometrical properties	Physical and mechanical properties*

	Cellulose (%)	Hémicellulose (%)	Lignin (%)	*l* (mm)	*d* (µm)	*l/d*	ρ ($g.cm^{-3}$)	E (GPa)	σ (MPa)
Flax	68.7–75.5	12.2–14	2.1–4.7	1.9 ± 0.02	27 ± 0.01	70.34	1.28–1.3	27–80	345–1830
Wood Pine	42	29	28	1.1 ± 0.02	32 ± 0.01	34.47	1.2	9	730

l: Mean length; d: Mean width; l/d: Aspect rtio; ρ : density; E: Young Modulus; σ : Stress.

* [31–37]

2.2. Accelerated aging test

Accelerated artificial aging was performed using a QUV/SE apparatus from Q-Lab Co., USA, with UVA-340 fluorescent lamps (UV irradiance at a wavelength of 340 nm) for a total of 960 h. Each aging cycle consisted of 8 h of dry UV exposure with an irradiance level of 1.55 W/m^2 at 60 °C. The changes in the surface color, roughness, surface morphology, flexural properties, and drop-weight impact behavior of the tested samples were evaluated after 0 h, 160 h, 320 h, 640 h, and 960 h.

2.3. The FTIR spectral measurements

Fourier transform infrared spectroscopy (Nicolet™ iS10 FTIR spectrometer) was used to study the surface chemical changes in the biocomposites before and during accelerated weathering. The scans were recorded with absorbance units of 650–4000 cm^{-1} at a resolution of 2 cm^{-1} to study the functional groups on the biocomposite surfaces. The measured spectra allowed for the analysis of the functional group modifications of the samples after UV aging.

2.4. Roughness measurements

The surface micro-topographies and roughness of the non-weathered and weathered samples were measured using a 3D laser confocal microscope (Keyence, Canada). The measurements allowed for the evaluation of the evolution of the sample roughness during the UV exposure using the average roughness parameter Ra.

2.5. Color analysis

The color evaluation of the unaged and aged samples was performed. The color was determined using a Nix Mini sensor according to the CIE 1976 system (L*, a*, b*); where L* (from 0–100) indicates a lightening material, and a* and b* are the positions of the chromaticity on the axes from -300 to +300, which are the green-to-red and blue-to-yellow axes, respectively. Given that

the L*, a*, and b* system is uniform, it allows for the calculation of the color difference between the non-weathered and weathered samples. The total color change (ΔE) was calculated in accordance with the ASTM D2244 standard using $\Delta E = \sqrt{\Delta L^2 + \Delta a^2 + \Delta b^2}$.

2.6. Three-point flexural test

Bending tests were performed using an Instron Model LM-U150 equipped with a 10 KN load cell, in accordance with the ASTM D790 standard [38] at a load speed of 1 mm/min. Three samples of each type were tested to verify the repeatability of the results. The deformation and strain were measured using a digital image correlation system (LaVision Inc., Göttingen, Germany).

The damage Mechanisms were continuously monitored during the bending test using an AE measurement system supplied by the Physical Acoustics Corporation (MISTRAS, USA). The AE signals were obtained using Micro-80 sensors (wideband, 100–1000 kHz), in which a silicone adhesive was employed as a coupling agent between the transducer and the specimen. To eliminate the background noise, the acoustic threshold was set as 35 dB. It should be noted that the quality of AE data depends on the AE wave parameters, namely, the peak definition time (PDT), hit definition time (HDT), and hit lockout time (HLT). The parameters were defined as PDT = 40 µs, HDT = 80 µs, and HLT = 200 µs. Before each test, a pencil break test procedure was used to calibrate the acquisition system and optimize the distance between the two sensors. The recorded AE acoustic signals were classified with respect to the amplitude, number of counts, duration, and frequency [3,38,39]. Based on the K-means clustering algorithm, each group of acoustic events was assigned to a damage mechanism.

2.7. Drop-weight impact test

Impact tests were performed in accordance with the ASTM D5628 standard using an Instron CEAST 9350 machine equipped with a 22-KN acquisition load cell. All samples were tested at a low impact energy of 2 J. We selected this low energy to study the influence on the material during UV-accelerated weathering. To verify the repeatability of the results, three samples were tested in each experiment, and the average of the results was considered for interpretation. After the tests, the cracks and damages in the impacted samples were measured using X-ray tomography.

3. Results and Discussion

3.1. Fourier transform infrared spectroscopy analysis

The FTIR spectra (600-2000 cm^{-1}) of SNFT PP30/F and PP30/P are shown in Figure 1. Spectral analysis revealed that the chemical structures of both SNFTs did not change after aging, given that the same characteristic bands typical of the original bands (unaltered SNFT) were observed. Nevertheless, after ageing, peaks 1315 cm^{-1} and 1420 cm^{-1} attribute to (O-H in plane bending of cellulose and hemicellulose) as well as peaks 1050 cm^{-1} and 1152 cm^{-1} attribute to (C2-O2H stretching of cellulose and hemicellulose) and (C1-O- C4 antisymmetric stretching of cellulose and hemicellulose) respectively increased as a function of exposure time suggesting the appearance of cellulose and hemicellulose in the photo-oxydation of biocomposites [40,41]. However, the photo-oxidation of the composites under UV irradiation can be mainly attributed to the carbonyl and carbon reactions of lignin, which correspond to the peaks at 1640 cm^{-1} and 1731 cm^{-1} [21,42]. Based on the results, the intensity of both peaks at 1640 cm^{-1} (absorbed O-H and conjugated C–O of lignin) and 1731 cm-1 (C=O stretching af acetyl or carboxylic acid of lignin) in both SNFTs increased during aging. After 960 h of exposure, the intensity of the peaks at 1640 cm^{-1} and 1731 cm^{-1} reached 40% and 125%, respectively, for PP30/F; and 128% and 275%, respectively, for PP30-P. These results suggest that pine fibers (rich in lignin) undergo more photo-oxidation reactions under UV irradiation. The presence of such bands before aging in the two SNFTs was due to the presence of carbonyl and carbon double bonds in cellulose, and especially the lignin of natural fibers [42].

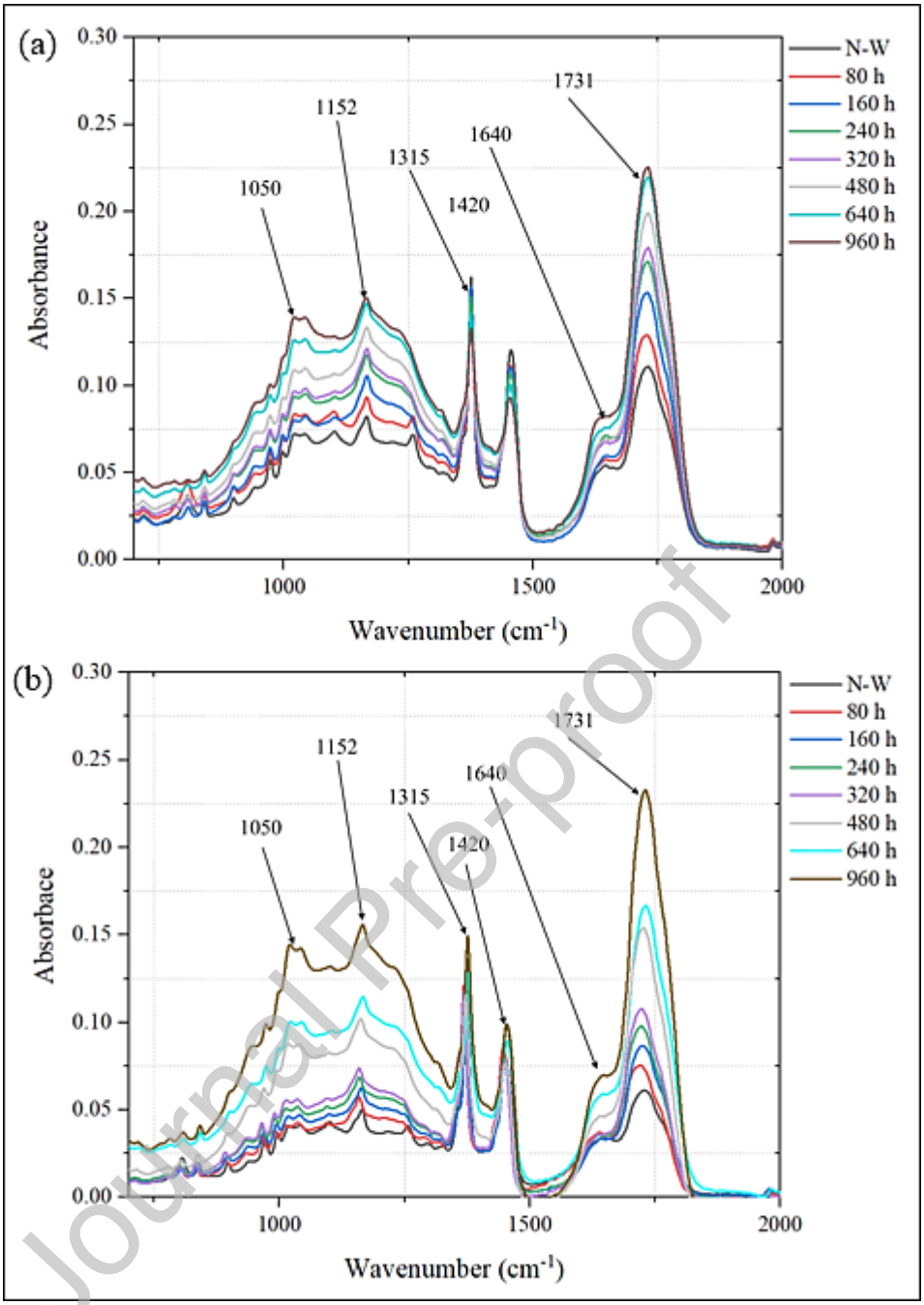

Figure 1. Infrared spectra of unaltered and altered samples: a) PP30-F and b) PP30-P.

3.2. Color measurement

The results in Figure 2 present the decoloration of PP30-F and PP30-P as a function of the exposure time. The results revealed that the color change ΔE of the two materials evolved

significantly within the first 480 h of exposure, and slight changes were recorded until 960 h. Hence, the change reached its maximum. These changes were attributed to a significant increase in the luminosity parameter (L value). Quantities a and b exhibited a small decrease for both materials (figure 2). An analysis of the images in Figure 2-d revealed that both materials exhibited significant color changes. The two materials were photobleached and illuminated after 960 h of UV exposure. The changes in the color of the biocomposites are mainly due to the loss of the methoxyl content of the lignin, the photo-dissociation of the carbon-carbon bonds and the formation of carbonyl-based chromophore groups [23]. According to the results the PP30-P are lighter, and they have a greater clarity L* in the initial state (before aging), reflecting a color difference DE * lower than PP30-F after ageing. This can be explained by the fact that the color of the natural fiber reverts to the rate of quinone structures including anthraquinones, naphthoquinones, phenanthraquinones and benzoquinones from lignin[43], and that Pine and Flax fibers has a different lignin structure[44,45], therefore the color properties will be different in the two natural fibres. It is known that lignin mainly consists of a compound of three types of substituted phenols, which include: p-hydroxyphenyl (H), vanillin (G), syringaldehyde (S)) [43]. In the case of Pine fibres, the G unit represents more than 90% of its lignin structure[45] while the Flax fibers contain 72% G unit, 13% H unit and 15% S-unit [44]. After 960 h of exposure, the color changes reached 40.95% and 31.31% for PP30-F and PP30-P, respectively.

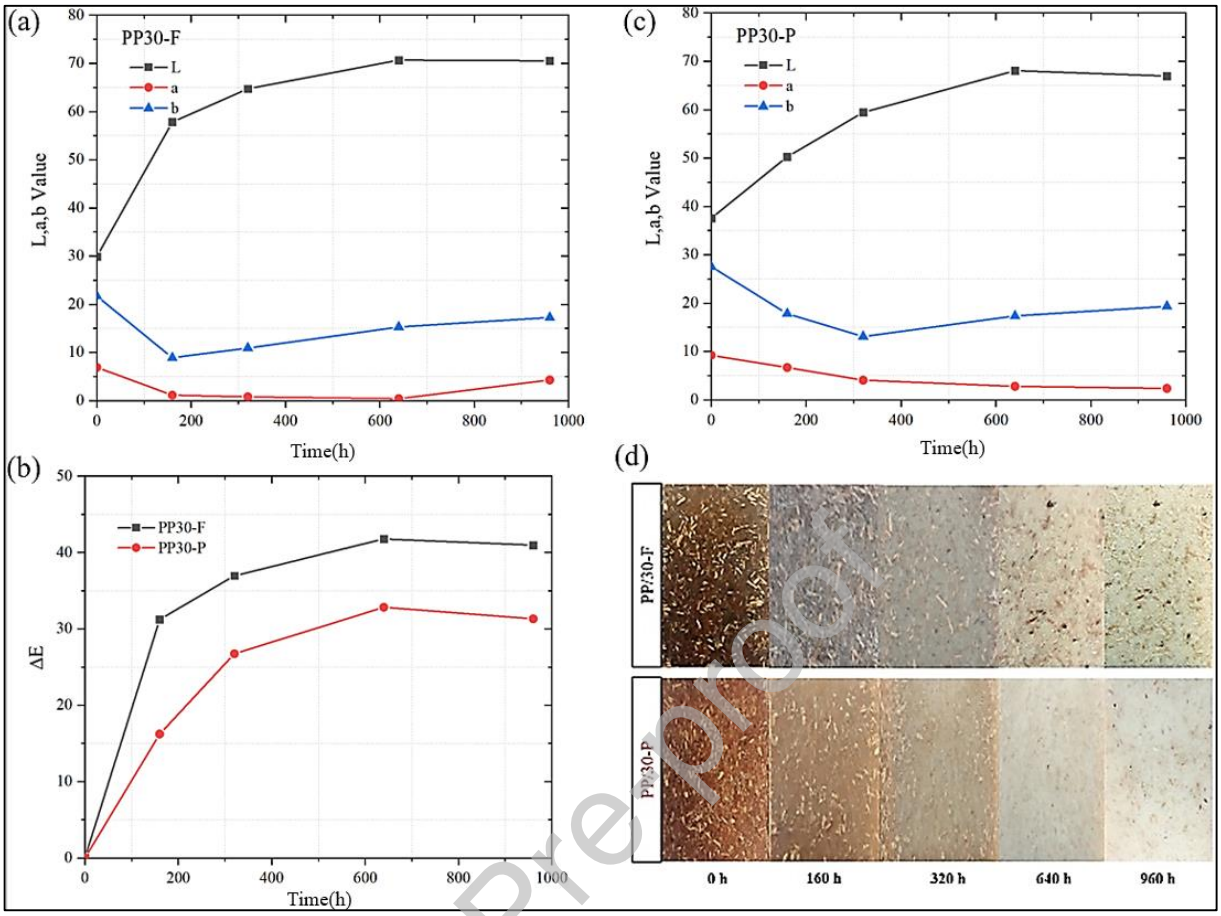

Figure 2. Evolution of the changes in color and luminosity as a function of the exposure time of Biocomposites PP30-F and PP30-P: a) L,a,b color change of PP30-F, b) L,a,b color change of PP30-P, c) total color changes iof PP30-F and PP30-P, and d) image color changes of PP30-F and PP30-P.

3.3. Roughness measurement

Figures 3 and 4 present the micro-topographies of the samples during aging. Before aging, both biocomposites exhibited defect-free and smooth surfaces. After 960 h of exposure, micro cracks were observed. The cracks were mainly due to the splitting of the chains of the PP matrix [23]. However, the phenomenon was less significant for PP30-P (contains more lignin) when compared with PP30-F, which can be attributed to the antioxidant effect of lignin [23]. Moreover, the profiles of the surface samples were indicated in the same figure.

The evolution of the average roughness of the PP30-F and PP30-P samples as a function of the exposure time is presented in Figure 5. An analysis of the results revealed that the roughness increased as a function of the exposure time for both materials. The increase in roughness can

be attributed to the increase in the duration of exposure of the biocomposites to UV irradiation, thus leading to photo-oxidation; in addition to the scission of the polymer chain and surface microcracks [21,42]. The appearance of these led to an increase in the roughness of the biocomposites [23]. Moreover, PP30-P exhibited relatively fewer rough surfaces, which may be due to the antioxidant effect of lignin. On average, pine fibers contain more lignin than flax fibers by a factor of 10 (Table 1). After 960 h of exposure, the PP30-F exhibited an Ra of 17.86 um when compared with that of 9.07 um for PP30-P.

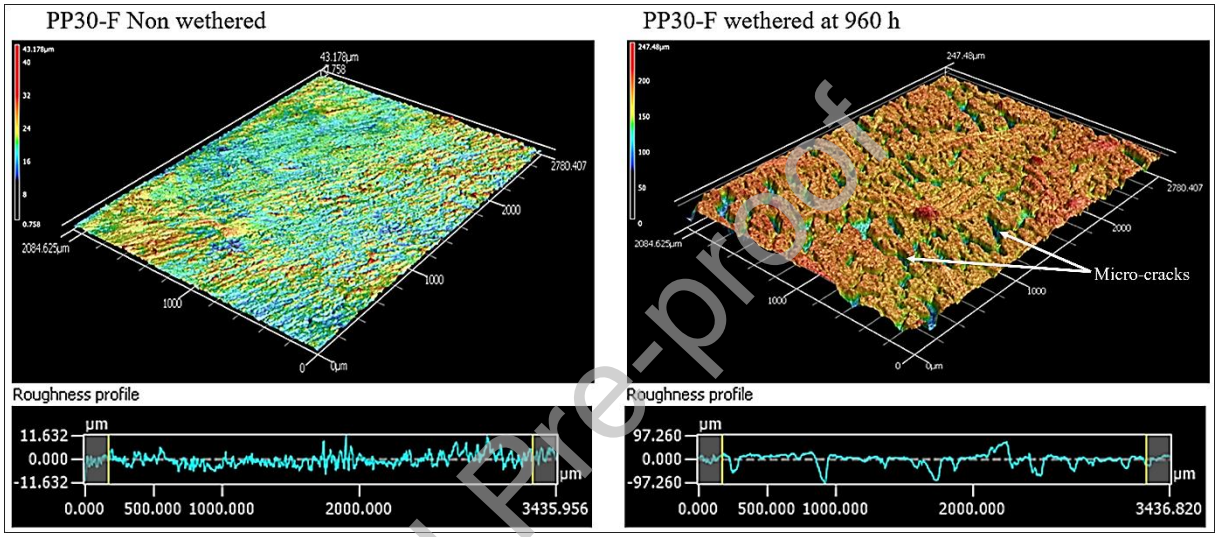

Figure 3. Topography surfaces and roughness profiles of unaltered and altered PP30-F samples at 960 h.

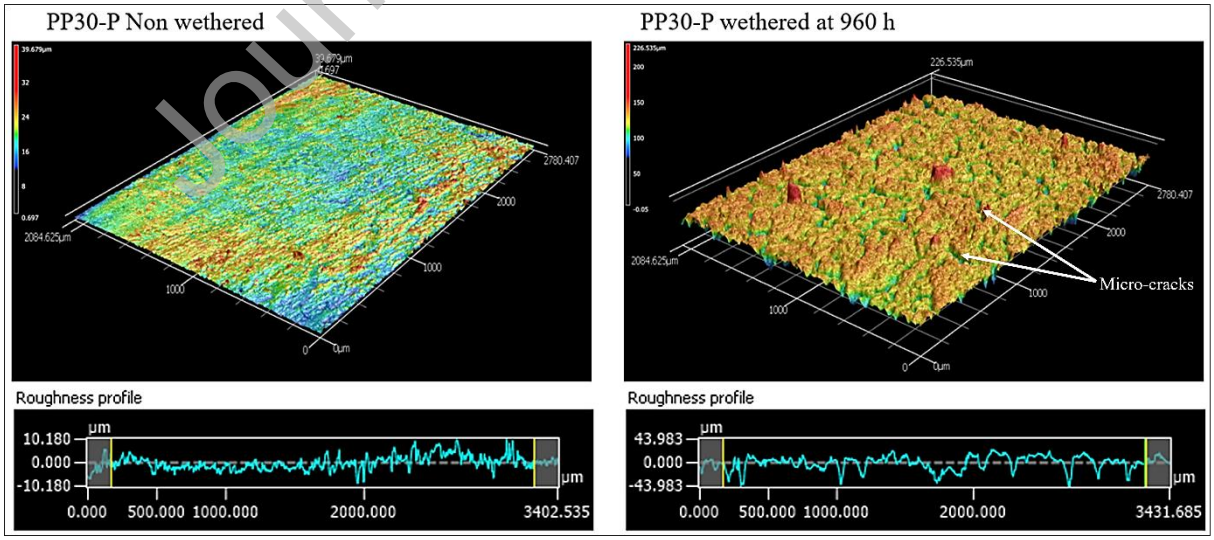

Figure 4. Topography surfaces and roughness profiles of unaltered and altered of PP30-P samples at 960 h.

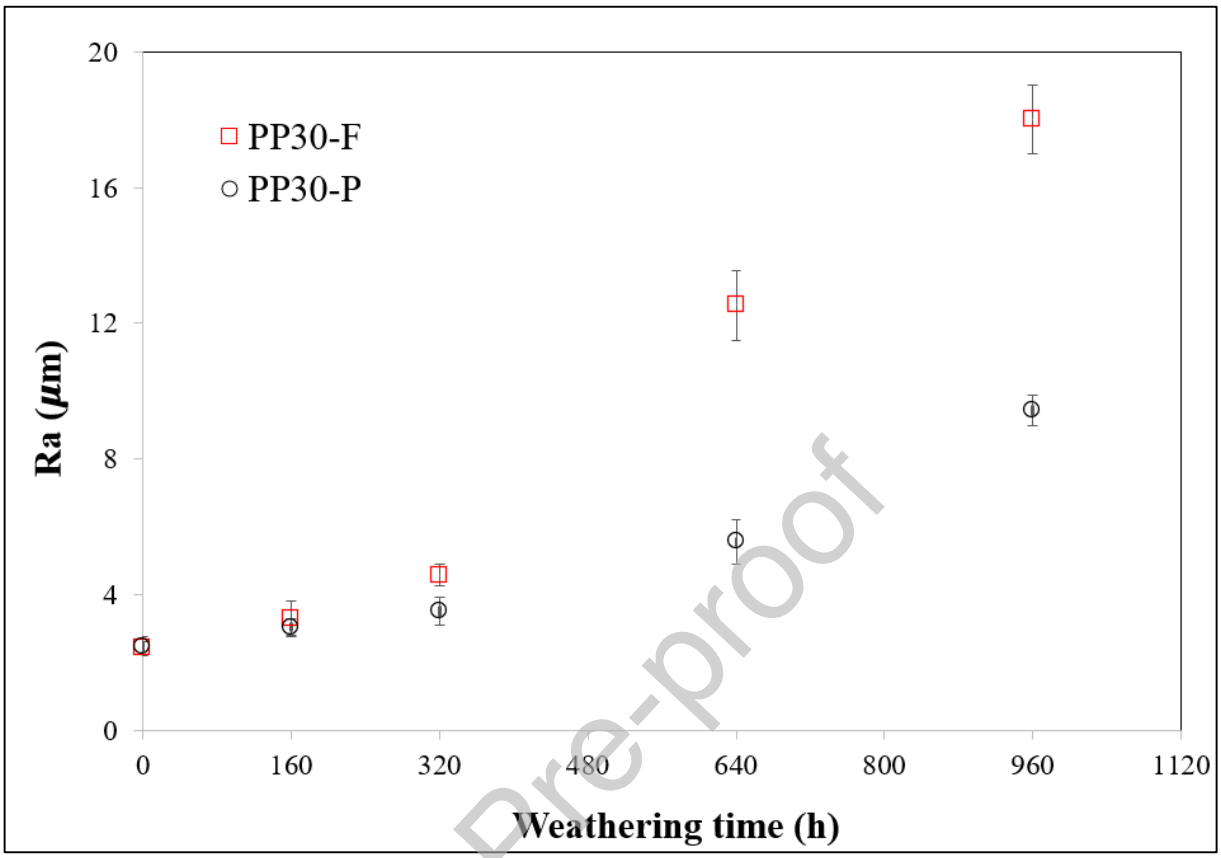

Figure 5. Mean roughness (Ra) evolution of PP30-Fand PP30-P as a function of the exposure time.

3.4. Bending test

Figure 6 presents the stress–strain curves of all the PP30-F and PP30-P samples. An analysis of the results revealed that the mechanical behavior of SNFT occurred in two phases: elastic linear behavior followed by a nonlinear part (plastic deformation and damage) until the fracture of the material. A decrease in mechanical properties was recorded for the altered specimens. This decrease can be attributed to the appearance of surface anomalies (microcracks), which amplified the local stresses thereby reducing the mechanical resistance of the material.

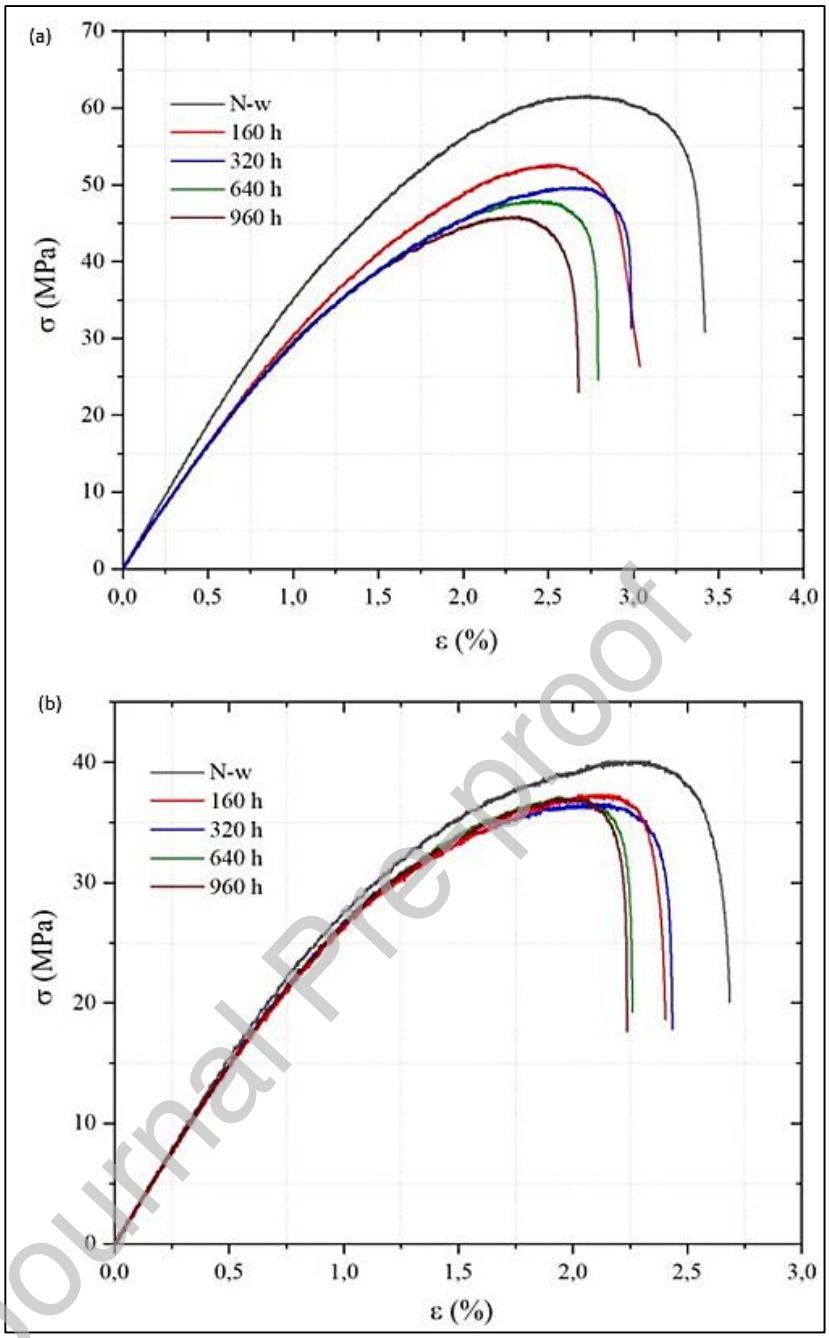

Figure 6. Bending test results for unaltered and altered samples a) PP30-F, b) PP30-P.

Figure 7 presents the degradation of the mechanical properties in bending: stiffness, mechanical resistance, and strain at break (ε_b) of the PP30-F and PP30-P biocomposites as a function of the exposure time to UV radiation. Before aging, PP30-F exhibited a Young's modulus, mechanical strength, and strain at break greater than those of PP30-P by 15%, 20%, and 5%, respectively. This suggests that fibers containing more cellulose and hemicellulose (flax) impart superior mechanical properties. Moreover, the difference can be attributed to the L/D ratio, in that fibers have a ratio twice as large as that of pine fibers, as shown in Table 1. As is common knowledge, a large aspect ratio yields an improved fiber adhesion matrix, thus reflecting the excellent

mechanical properties of biocomposites [46]. When the samples were exposed to UV radiation, all properties of both biocomposites were degraded due to surface oxidation, changes in matrix crystallinity, and interfacial degradation [47]. The mechanical properties of both biocomposites were degraded, with a significant decrease in the first 480 h, followed by a slight decrease after 960 h of exposure. In particular, the rate of decrease in PP30-F was greater; thus, it was more sensitive than PP30-P. This can be attributed to the antioxidant effects of lignin. Peng et al 2015 [16] noted that lignin induced a smaller decrease in the flexural strength and Young's modulus of SNFT.

The mechanical bending properties of the unaltered and altered biocomposites at 960 h and the percentage loss of each property are listed in Table 2. The results revealed the high reproducibility of the measurements with a low standard deviation. Before aging, the PP30-F samples exhibited relatively superior properties (E_b = 3.64 GPa, σ_b = 61.55 Mpa, ε_b = 3.44%) to those of PP30-P (E_b = 3.29 Gpa, σ_b = 40.11 Mpa, ε_b = 2.68%). However, they underwent more degradation after 960 h of exposure, with a significant decrease of 17.03% in E_b, 26.43% in σ_b, and 23.83% in ε_b; whereas, those of PP30-P decreased by 9.72%, 9.70%, and 17.53%, respectively.

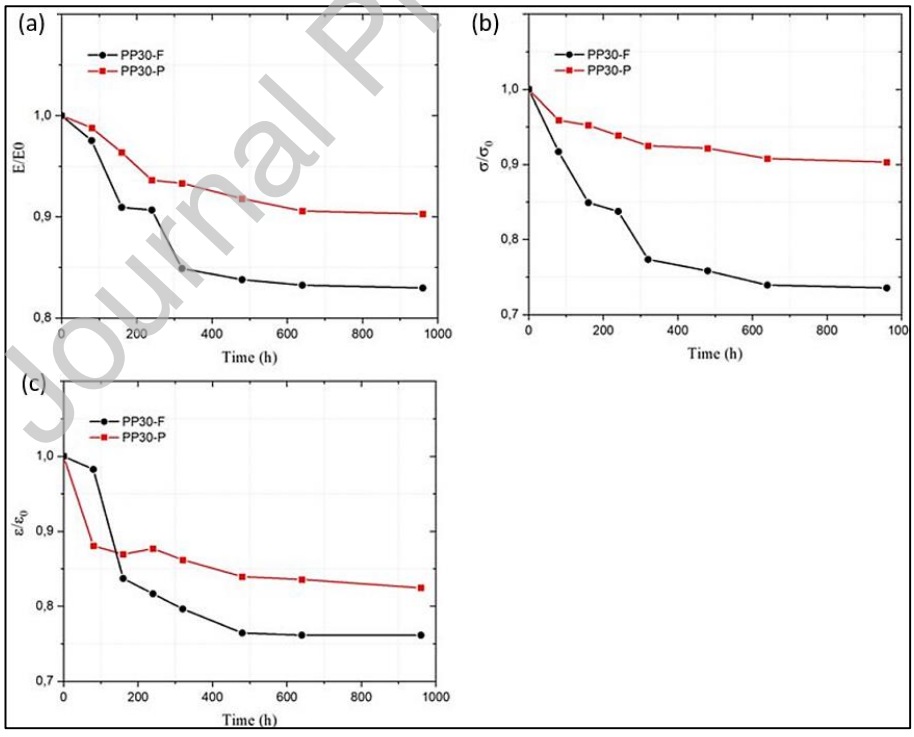

Figure 7. Evolution of mechanical bending properties of PP30-F and PP30-P on normalized axes: a) bending modulus (E_b), b) flexural strength (σ_b), and c) deformation at failure (ε_b).

Table 2. Flexural properties of composites before and after 960 h weathering

Materials	Conditions	Flexural properties		
		E_b [Gpa]	σ_b [Mpa]	ε_b [%]
PP30/F	Unweathered	3.64 (4.94)	61.55 (2.85)	3.44 (0.29)
	Weathered for 960 h	3.02 (2.98)	45.28 (2.38)	2.62 (0.76)
	Difference [%]	17.03	26.43	23.83
PP30/P	Unweathered	3.29 (2.43)	40.11 (2.79)	2.68 (0.75)
	Weathered for 960 h	2.97 (3.70)	36.22 (2.78)	2.21 (0.45)
	Difference [%]	9.72	9.70	17.53

E_b: Bending modulus; σ_b: Flexural strength; ε_b: Deformation at failure.
Values in parentheses are standard deviations.

The cumulative AE energy and crack propagation were recorded using two acoustic sensors and a digital image correlation system, respectively, to investigate the damage evolution and its contribution to the behavior of the biocomposites. The crack evolution during the test is shown in Figures 8 and 9. Before aging, during flexure, the stress–strain curves of the two materials exhibited a linear region, in which no AE activity or crack propagation was recorded. The slopes of the stress–strain curves of PP30-F and PP30-P then decreased from 0.65% and 0.72%, respectively. The first acoustic emission burst was then detected, and the AE energy increased slightly until strains of 2.7% and 2.25% were reached for PP30-F and PP30-P, respectively, thus indicating damage and plastic deformation until the maximum flexure strength point. Finally, the stress–strain curves decreased rapidly, and the AE energy curve was exponential, thus indicating the propagation of macrocracks prior to the final failure.

Similar to the results obtained for the unweathered samples, the weathered PP30-P sample at 320 h exhibited a linear region, followed by a non-linear region, and then a rupture phase (crack propagation). However, the second phase was within the strain range of 0.6–1.8%. This discrepancy can be attributed to the presence of superficial microcracks in the biocomposites due to photo-oxidation, which led to indications of damage when compared with the unaged samples. Figure 10 presents the scanning electron microscopy (SEM) images, which allows for the visualization of the surface states of the samples before the bending test.

However, when PP30-F was exposed for 320 h, PP30-P and PP30-F exposed for 960 h exhibited different results to those obtained previously, in that the behavior of the materials was first linearly elastic. However, the AE energy increased from the start of loading, thus suggesting

that indications of damage were recorded. This can be attributed to the increase in size of the superficial microcracks (figure 10), which then propagated under the influence of weak mechanical stresses. This propagation of superficial microcracks led to the recording of the indications of damage during the linear phase. Thereafter, the slopes of the stress–strain curves decreased in parallel, and those of the AE energy curves increased slightly, thus indicating the start of the second viscoelastic phase. The second phase extended to 2.4%, 1.9%, and 2.6% deformation for PP30-F altered at 320 h, PP30-F altered at 960 h, and PP30-P altered at 960 h, respectively. Finally, a downward shift in the stress–strain curves corresponded to an exponential increase in the AE energy. Similarly, the crack–strain curve increased exponentially, thus indicating the total rupture of the specimens.

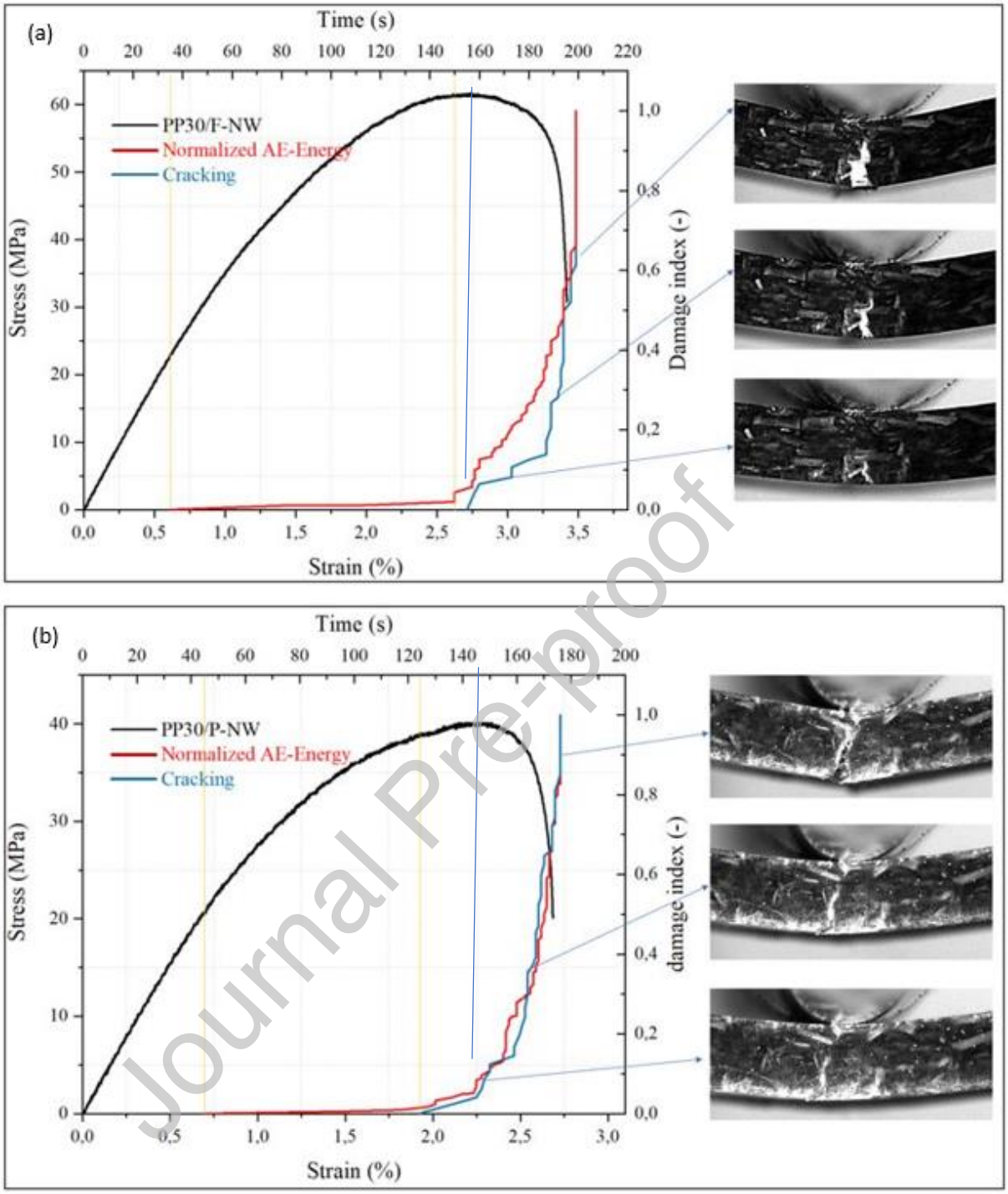

Figure 8. a) Correlation between the stress–strain curves and the normalized acoustic emission energy, and b) correlation between the stress–strain curves and the evolution of the normalized crack length in the bending tests of the unaltered PP30-F and PP30 -P biocomposites.

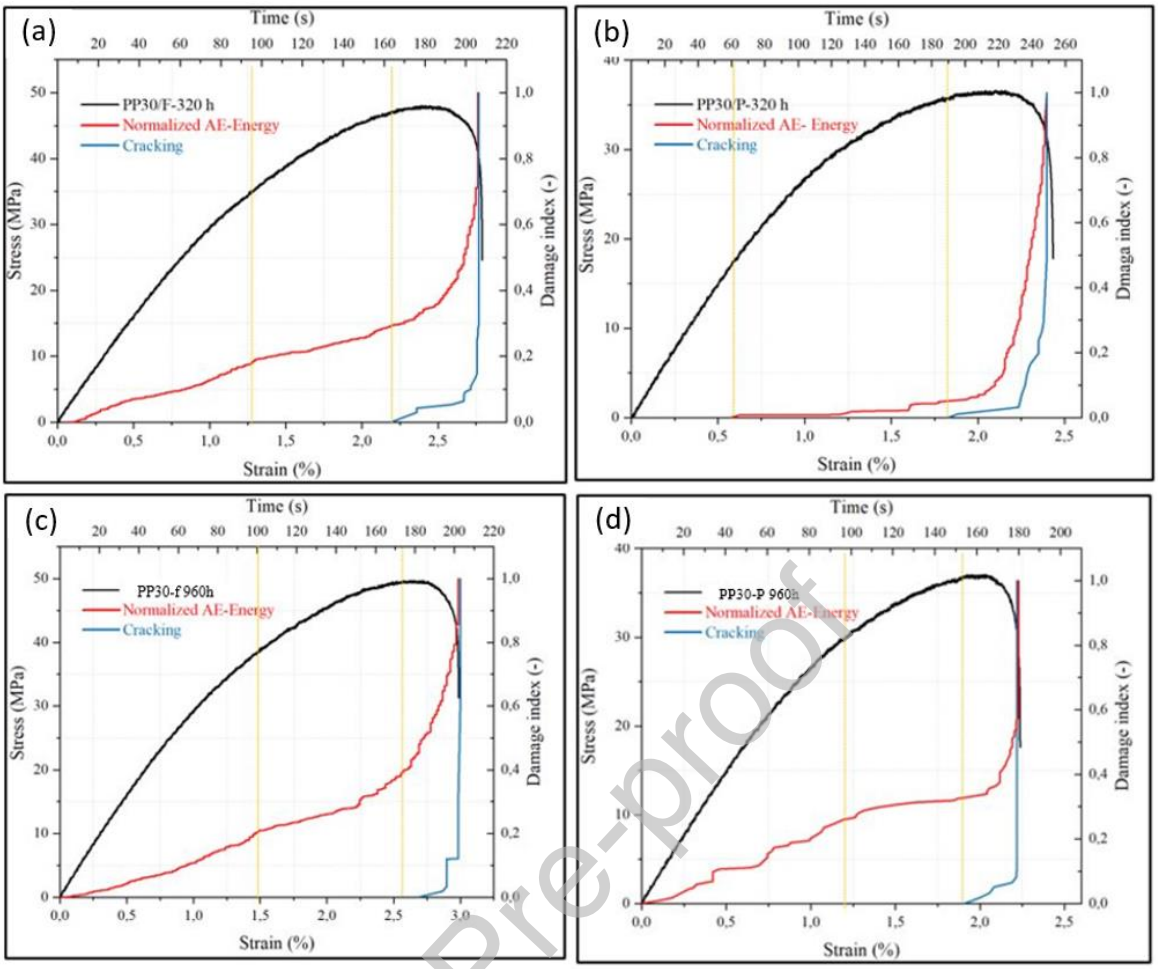

Figure 9 . Correlation between the stress–strain curves and the normalized AE energy, and correlation between the stress–strain curves and the evolution of the normalized crack length of the bending tests, respectively, for a) PP30-F altered at 320 h; b) PP30-P altered at 320 h; c) PP30-F altered at 960 h; and d) PP30-P altered at 960 h.

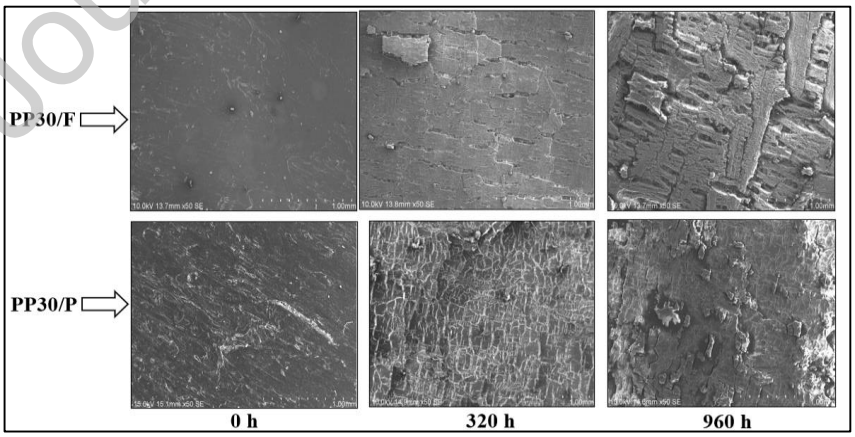

Figure 10 . The SEM images of the surfaces of the unweathered and weathered samples at 320 h and at 960 h.

3.5. Drop-weight impact test

Figures 11-a a and 11-b present the force–time responses of the PP30-F and PP30-P biocomposites (altered and unaltered). The responses of all the samples were bell-shaped. In addition, they exhibited significant load drops, followed by high-amplitude oscillations. These correspond to the damage mechanisms of both biocomposites. The oscillations increased with an increase in the exposure of both materials to UV radiation. This is because the weathered biocomposites exhibited superficial microcracks (Figure 10). These microcracks caused more damage to the biocomposites during impact loading. The first drop in the curves corresponds to the critical load F_c and indicates the start of material damage. Moreover, the variation and increase in energy beyond this point was due to the initiation and propagation of microcracks in the biocomposites [28,29]. These microcracks decreased the rigidity and strengths of the materials. In addition, there was a significant drop in load, which coincided with the maximum force in the force–time curves from 320 h and 640 h of exposure for PP30-F and PP30-P, respectively. In general, this decrease corresponds to an accumulation of cracks, or significant loss in the mechanical resistance of the material [29]. Furthermore, the response time increased as a function of the exposure time for both materials.

During the testing of all the samples, the striker rebounded with the elastic energy stored in the samples. This indicates that the impact behavior of the samples was not perforation. The energy absorbed by the samples can be calculated as the area between the loading and unloading parts of the force–displacement curve. The force–displacement curves of Biocomposites PP30-F and PP30-P (altered and unaltered) are presented in Figures 12-a and 12-b. With respect to the data, the area between the loading and unloading parts increased slightly as a function of the exposure time in both biocomposites. This indicated that the material absorbed more energy. Similarly, the maximum displacement increased as a function of the exposure time for both materials.

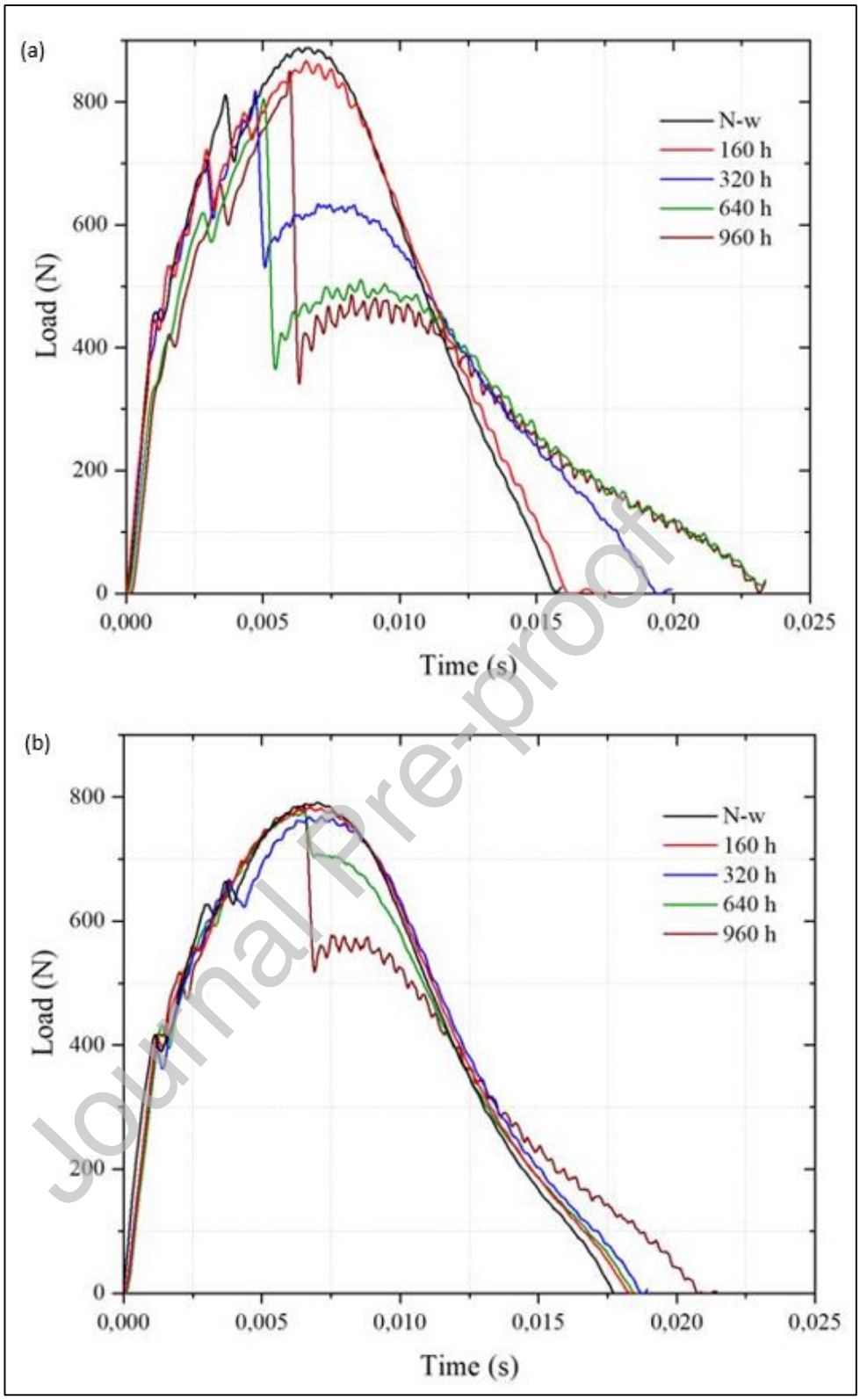

Figure 11. Load-time response of altered and unaltered biocomposites: a) PP30-F and b) PP30-P.

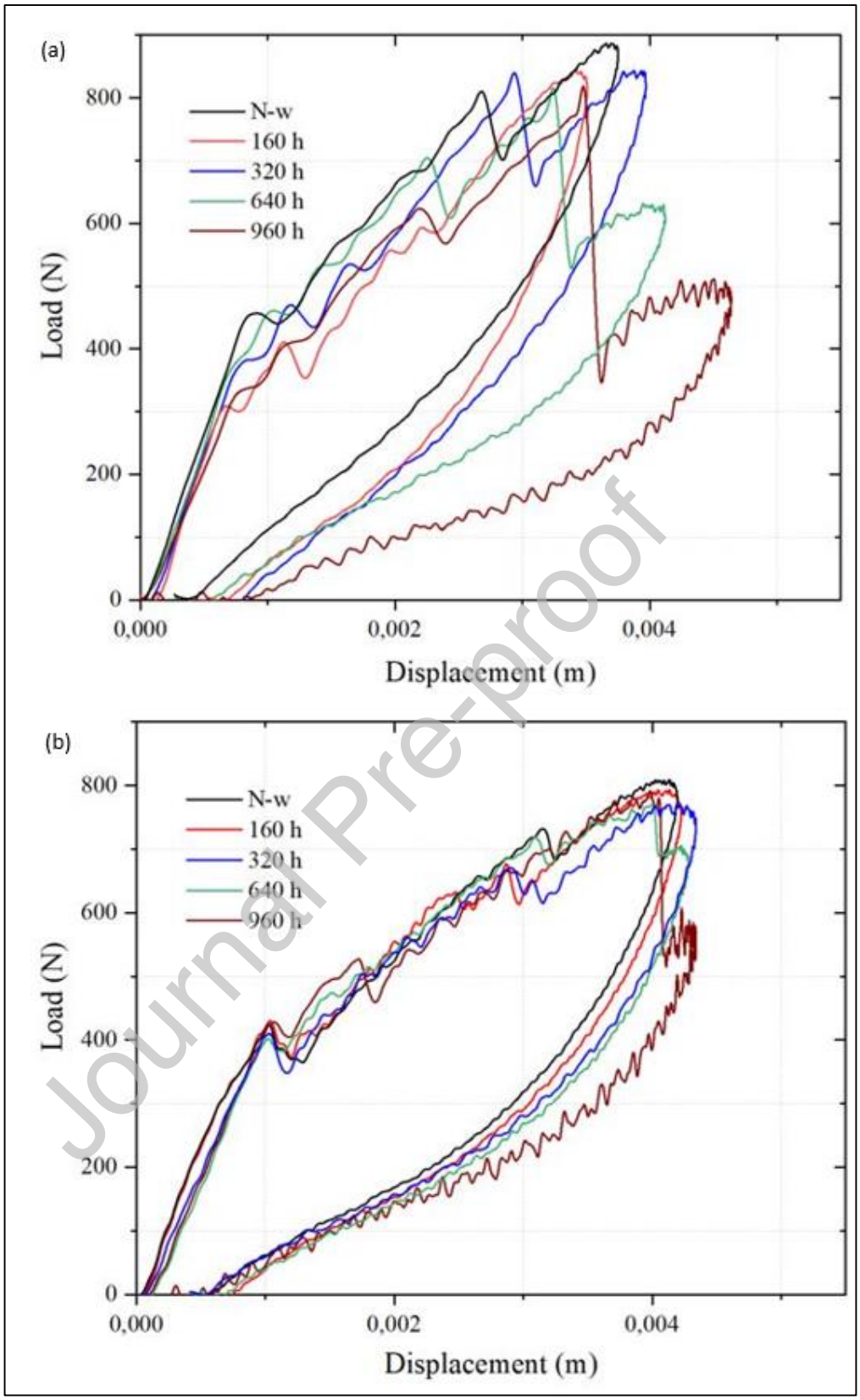

Figure 12. Load-time response of altered and unaltered biocomposites a) PP30-F and b) PP30-P.

Figure 13 shows the evolution of the impact properties of PP30-F and PP30-P as functions of the exposure time. The analysis of the results revealed that, for both materials, the critical force and maximum force decreased in accordance with an increase in the exposure time, in parallel; and the deformation and absorbed energy increased. This was similar to the results obtained from the bending tests (Figure 7). Compared with PP30-P, the degradation rate of PP30-F was higher, especially within 480 h of exposure. This can be primarily attributed to the surface conditions of the samples, in which PP30-F exhibited more significant surface damage, as previously mentioned (Figure 10).

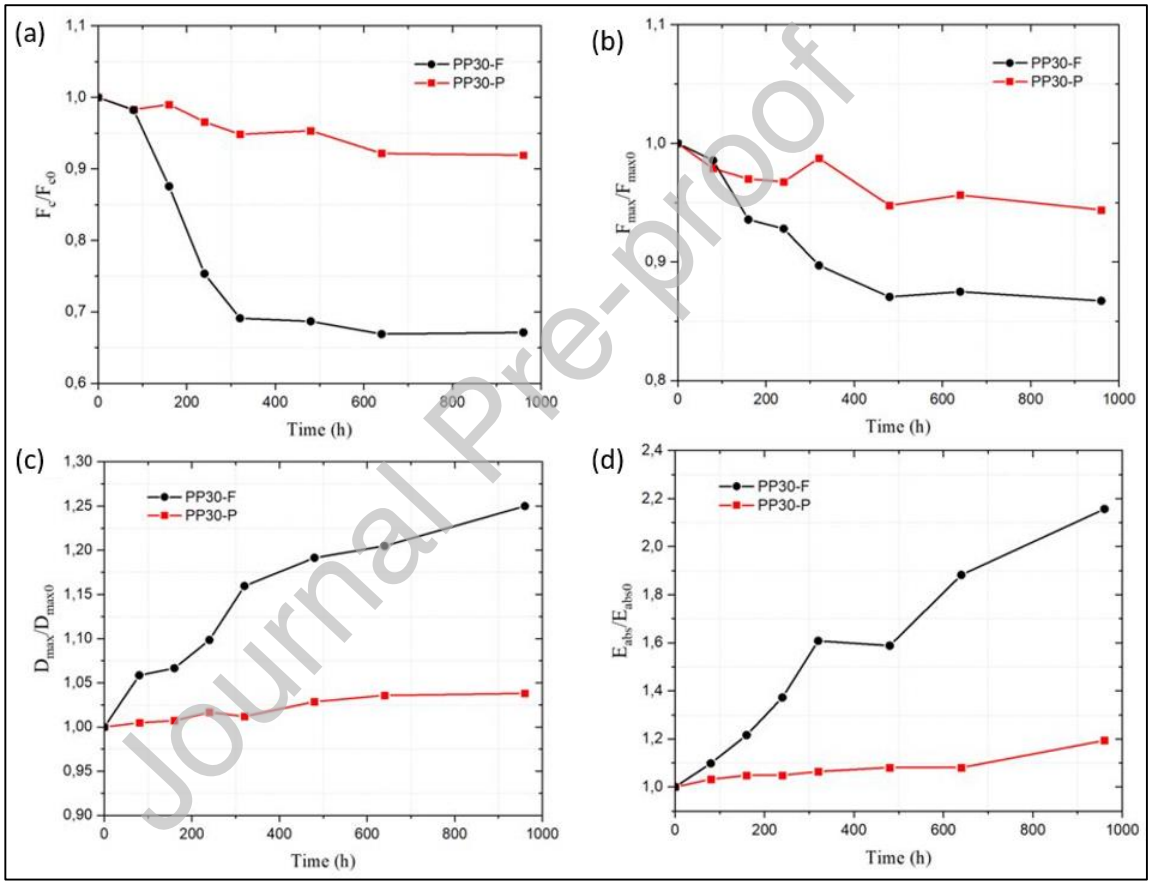

Figure 13. Impact property evolution of PP30-F and PP30-P (unaltered and altered samples).

Table 3 lists the impact properties (F_c, F_{max}, D_{max}, and E_{max}) of the unweathered and weathered biocomposites at 960 h, in addition to the percentage decrease in each property. The results exhibited a high reproducibility of the measurements with a low standard deviation. Before alteration, when compared with PP30-P, PP30-F exhibited the maximum resistance and a greater critical force. However, the PP30-F samples were relatively less deformable and

absorbed less energy. In particular, F_c = 450 N, F_{max} = 900 N, D_{max} = 5 mm, and E_{abs} = 0.5 J were obtained for PP30-F; and F_c = 420 N, F_{max} = 850 N, D_{max} = 6 mm, and E_{abs} = 0.64 J for PP30-P. The difference in properties between the two biocomposites can be primarily attributed to the difference in the chemical and physical properties of each fiber (Table 1). After 960 h of exposure, PP30-F exhibited greater degradation than PP30-P. The degradation of PP30-F was 33% of F_c, 13% of F_{max}, 25% of D_{max}, and 52% of E_{abs}; which respectively corresponded to 10%, 5%, 4%, and 24% for PP30-P.

Table 3. Impact properties of composites before and after weathering for 960 h

Materials	**Conditions**	**F_c [N]**	**F_{max} [N]**	**D_{max} [mm]**	**E_{ab} [J]**	**T [s]**
P 30/F	Unweathered	450.31 (1.13)	903.78 (1.15)	3.76 (2.92)	0.51 (1.96)	15.82 (3.22)
	Weathered for 960 h	302.75 (2.76)	783.25 (1.64)	4.70 (1.70)	0.96 (1.04)	23.97 (2.75)
	Difference [%]	32.77	13.34	25	88.24	51.52
PP30/P	Unweathered	418.01 (1.11)	802.44 (1.37)	4.20 (6.36)	0.62 (1.61)	17.14 (2.45)
	Weathered for 960 h	375.38 (2.56)	757.11 (2.07)	4.36 (2.75)	0.74 (1.35)	21.23 (3.25)
	Difference [%]	10.19	5.64	3.8	19.35	23.86

F_c: critical load; F_{max} : maximum load; D: maximum displacement; E_{ab}: absorbed energy; T: time.

Values in parentheses are standard deviations.

The damage induced by the impact of the unweathered and weathered biocomposites at 320 h and 960 h are presented in Figures 14 and 15, respectively. The cracks exhibited X shapes at the centers of the specimens; or were occasionally random, as in the case of the samples altered at 960 h, due to the heterogeneous nature of the biocomposites. The sizes of the cracks increased in accordance with an increase in exposure time for both materials. Moreover, the cracks were surrounded by microcracks. This may be due to the vacuums within the samples. However, in the case of the aged samples, the numbers and sizes of microcracks become important. This may be due to the increase in the sizes of the superficial cracks due to aging in accordance with an increase in the exposure time, thus leading to microcrack propagation under impact action. An increased number of voids was therefore observed.

Table 4 presents the void percentages of all impacted samples. Based on the data, the void ratio increased as a function of the exposure time for both materials. Moreover, irrespective of the exposure time, the PP30-F samples exhibited more voids than the PP30-P samples. This indicates that PP30-F was more damaged.

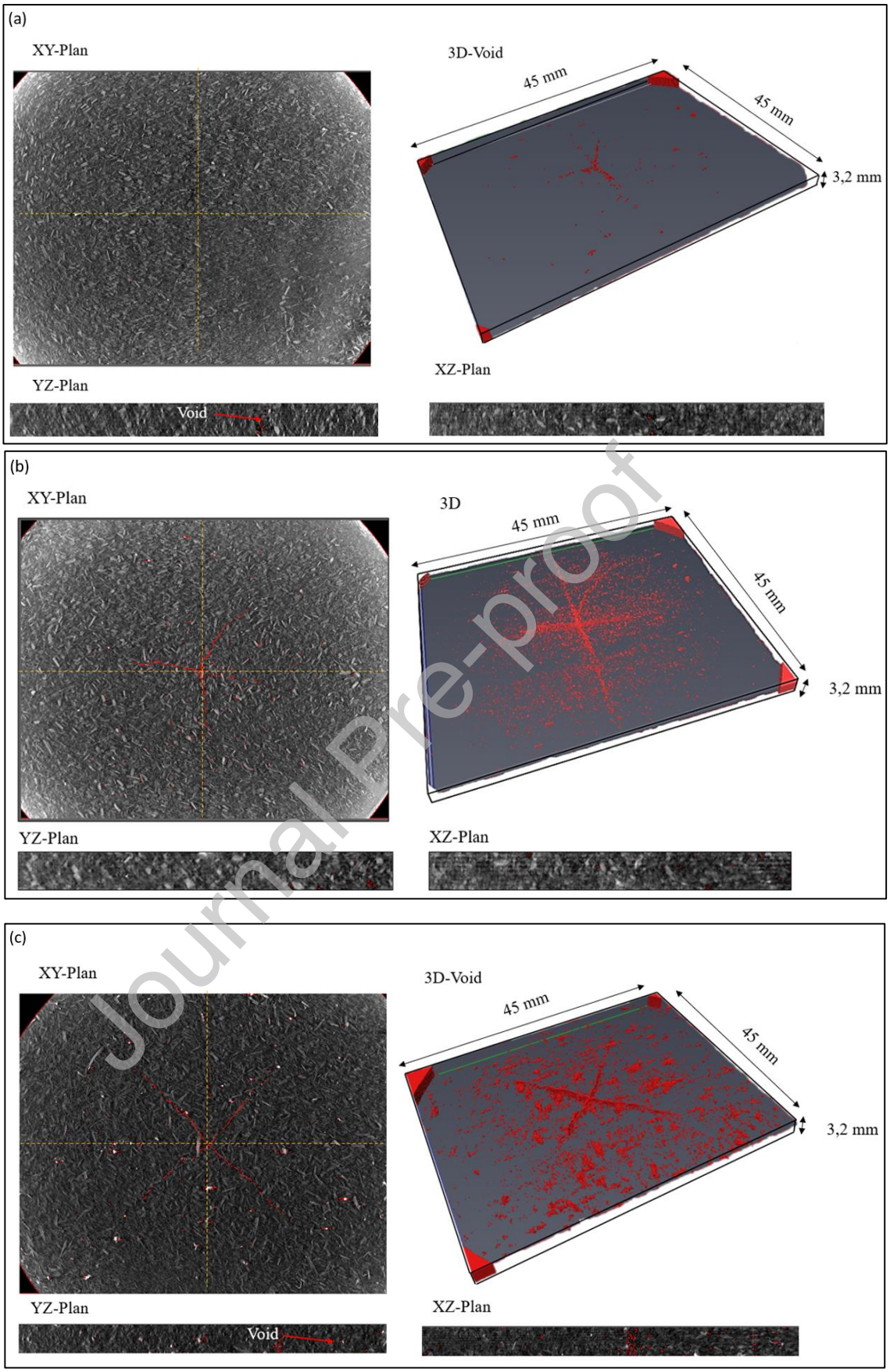

Figure 14. Tomography image of impacted PP30-F samples: a) non-weathered, b) weathered at 320 h, and c) weathered at 960h.

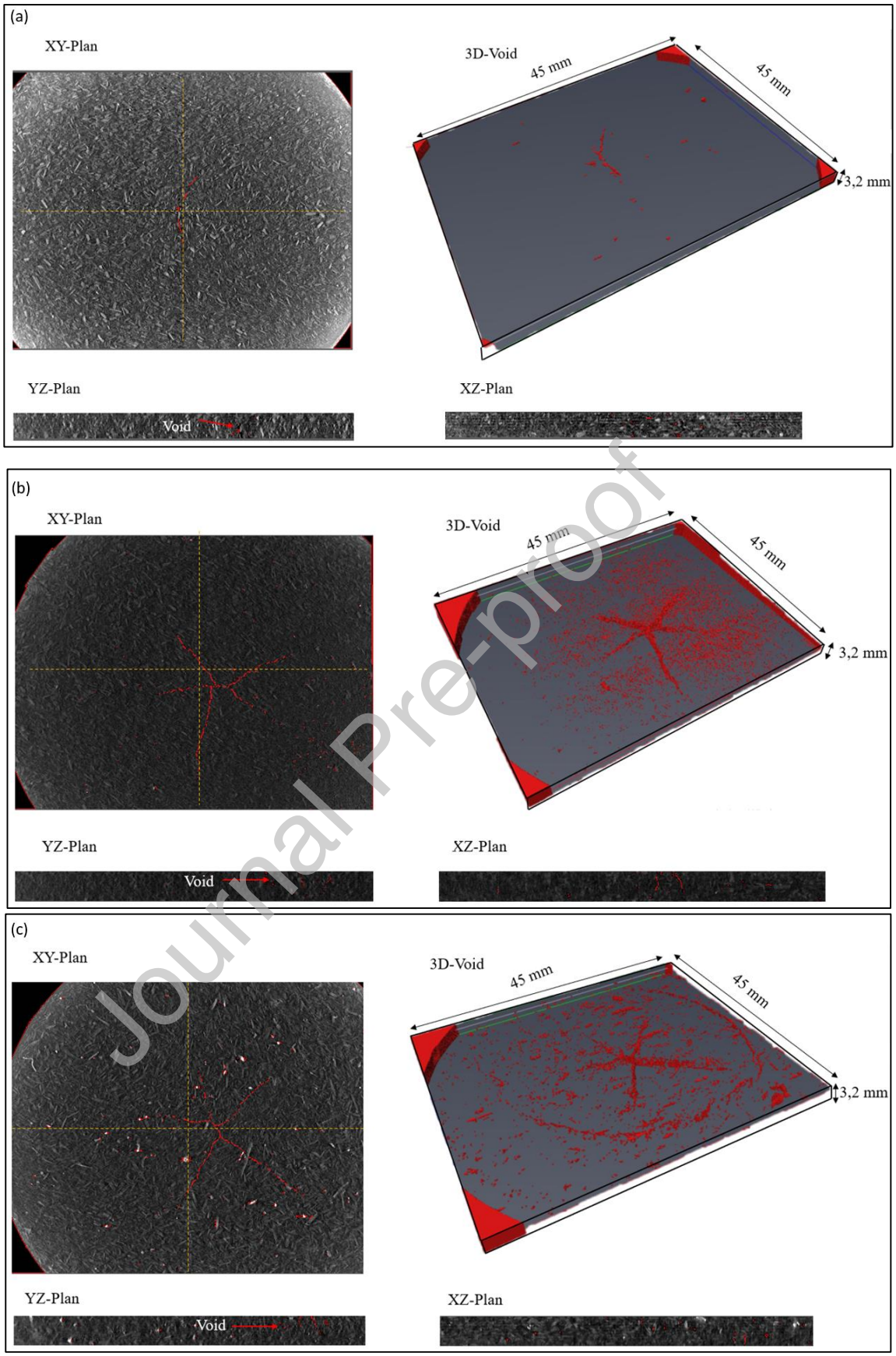

Figure 15. Tomography image of impacted PP30-P samples: a) non-weathered, b) weathered at 320 h, and c) weathered at 960 h.

Table 4. Percentage of voids in impacted PP30-F and PP30-P samples

Samples	**Damage (%)**				
	Non weathered	**160 h**	**320 h**	**640 h**	**960 h**
PP30-F	8.26 %	9,11 %	15,34 %	16,89 %	18,38 %
PP30-P	7.41 %	7,98 %	12,27 %	14,52 %	15,14 %

4. Conclusions

In this study, two types of natural fibers, namely, flax fibers and pine fibers, which are used as reinforcements for a polypropylene-based composite, were compared in terms of durability under UV irradiation. Changes in the chemical structure, color, roughness, and mechanical properties of the biocomposites under UV irradiation were evaluated using FTIR, colorimetry, and confocal laser imaging; in addition to bending and drop-weight impact tests. The damage behavior was tracked during the bending tests using the AE technique, and the damage due to the impact was evaluated using computerized tomography (CT) scan measurements.

It appears from the analysis of the results that lignin promotes photo-oxidation reactions in biocomposites, in which more photo-oxidation reaction was recorded by PP30-P samples than by PP30-F. since Pine fiber contains more lignin in its chemical structure. Otherwise, the color of the two biocomposites turns almost white after 960 hours of exposure after they were dark. Indeed, PP30-F exhibited a relatively large color change due to the difference in the chemical composition of the lignin in the two fibers. In addition, the antioxidant effect of lignin dampened the propagation of surface cracks in PP30-P. This damping reflects PP30-P specimens with relatively less rough surfaces.

Bending tests revealed that flax fibers contain more cellulose in their chemical structure and exhibit a relatively larger geometric ratio (almost twice that of pine fibers) resulting in stiffer and stronger composites. However, after aging, PP reinforced with pine fiber exhibited a relatively lower degradation rate. Since PP 30-P has fewer surface cracks than PP30-F and therefore less stress concentration. Otherwise, the AE analysis revealed that the decrease of the mechanical properties of the composites under UV irradiation is mainly related to the number and sizes of surface cracks.

Otherwise, the results of the impact tests confirmed the results obtained from the bending tests in terms of the resistance. Before aging, PP30-F had a relatively higher impact resistance; however, after aging, more degradation was observed. In the case of both materials, the crack

undergoing impact increased in accordance with an increase in the exposure time, during which the propagation was more critical in PP30-F. This is because PP30-F exhibited more superficial cracks, thus crack propagation occurred more readily under impact loading. In addition, the study confirms that UV irradiation and damage mechanisms are highly material dependent.

References

[1] Pickering KL, Efendy MGA, Le TM. A review of recent developments in natural fibre composites and their mechanical performance. Compos Part A Appl Sci Manuf 2016;83:98–112. https://doi.org/10.1016/j.compositesa.2015.08.038.

[2] Andrew JJ, Dhakal HN. Sustainable biobased composites for advanced applications: recent trends and future opportunities – A critical review. Compos Part C Open Access 2022;7:100220. https://doi.org/10.1016/j.jcomc.2021.100220.

[3] Bravo A, Toubal L, Koffi D, Erchiqui F. Development of novel green and biocomposite materials: Tensile and flexural properties and damage analysis using acoustic emission. Mater Des 2015;66:16–28. https://doi.org/10.1016/j.matdes.2014.10.026.

[4] Nagaraja S, Bindiganavile Anand P, Mahadeva Naik RN, Gunashekaran S. Effect of aging on the biopolymer composites: Mechanisms, modes and characterization. Polym Compos 2022:1–11. https://doi.org/10.1002/pc.26708.

[5] Seldén R, Nyström B, Långström R. UV aging of poly(propylene)/wood-fiber composites. Polym Compos 2004;25:543–53. https://doi.org/10.1002/pc.20048.

[6] Beg MDH, Pickering KL. Accelerated weathering of unbleached and bleached Kraft wood fibre reinforced polypropylene composites. Polym Degrad Stab 2008;93:1939–46. https://doi.org/10.1016/j.polymdegradstab.2008.06.012.

[7] Kallakas H, Poltimäe T, Süld TM, Kers J, Krumme A. Kunstliku vanandamise mõju puitplastkomposiitide mehaanilistele ja füüsikalistele omadustele. Proc Est Acad Sci 2015;64:94–104. https://doi.org/10.3176/proc.2015.1S.05.

[8] Mejri M, Toubal L, Cuillière JC, François V. Hygrothermal aging effects on mechanical and fatigue behaviors of a short- natural-fiber-reinforced composite. Int J

Fatigue 2018;108:96–108. https://doi.org/10.1016/j.ijfatigue.2017.11.004.

[9] Stark NM, Matuana LM. Ultraviolet weathering of photostabilized wood-flour-filled high-density polyethylene composites. J Appl Polym Sci 2003;90:2609–17. https://doi.org/10.1002/app.12886.

[10] Sodoke FK, Toubal L, Laperrière L. Hygrothermal effects on fatigue behavior of quasi-isotropic flax/epoxy composites using principal component analysis. J Mater Sci 2016;51:10793–805. https://doi.org/10.1007/s10853-016-0291-z.

[11] Stark NM, Matuana LM. Influence of photostabilizers on wood flour-HDPE composites exposed to xenon-arc radiation with and without water spray. Polym Degrad Stab 2006;91:3048–56. https://doi.org/10.1016/j.polymdegradstab.2006.08.003.

[12] Toubal L, Zitoune R, Collombet F, Gleizes N. Moisture Effects on the Material Properties of a Jute/Epoxy Laminate: Impulse Excitation Technique Contribution. J Nat Fibers 2018;15:39–52. https://doi.org/10.1080/15440478.2017.1302389.

[13] Joseph P V., Rabello MS, Mattoso LHC, Joseph K, Thomas S. Environmental effects on the degradation behaviour of sisal fibre reinforced polypropylene composites. Compos Sci Technol 2002;62:1357–72. https://doi.org/10.1016/S0266-3538(02)00080-5.

[14] Pattamasattayasonthi N, Chaochanchaikul K, Rosarpitak V, Sombatsompop N. Effects of UV weathering and a CeO2-based coating layer on the mechanical and structural changes of wood/PVC composites. J Vinyl Addit Technol 2011;17:9–16. https://doi.org/10.1002/vnl.20246.

[15] Falk RH, Lundin T, Felton C. The effects of weathering on wood-thermoplastic composites intended for outdoor applications. Proc 2nd Annu Conf Durab Disaster Mitig Wood-Frame Hous 2001:175-179\r263.

[16] Peng Y, Liu R, Cao J. Characterization of surface chemistry and crystallization behavior of polypropylene composites reinforced with wood flour, cellulose, and lignin during accelerated weathering. Appl Surf Sci 2015;332:253–9. https://doi.org/10.1016/j.apsusc.2015.01.147.

[17] Soccalingame L, Perrin D, Bénézet JC, Bergeret A. Reprocessing of UV-weathered

wood flour reinforced polypropylene composites: Study of a natural outdoor exposure. Polym Degrad Stab 2016;133:389–98. https://doi.org/10.1016/j.polymdegradstab.2016.09.011.

[18] Belec L, Nguyen TH, Nguyen DL, Chailan JF. Comparative effects of humid tropical weathering and artificial ageing on a model composite properties from nano- to macro-scale. Compos Part A Appl Sci Manuf 2015;68:235–41. https://doi.org/10.1016/j.compositesa.2014.09.028.

[19] Thirmizir MZA, Ishak ZAM, Taib RM, Rahim S, Jani SM. Natural Weathering of Kenaf Bast Fibre-Filled Poly(Butylene Succinate) Composites: Effect of Fibre Loading and Compatibiliser Addition. J Polym Environ 2011;19:263–73. https://doi.org/10.1007/s10924-010-0272-2.

[20] Fabiyi JS, McDonald AG, Wolcott MP, Griffiths PR. Wood plastic composites weathering: Visual appearance and chemical changes. Polym Degrad Stab 2008;93:1405–14. https://doi.org/10.1016/j.polymdegradstab.2008.05.024.

[21] Badji C, Beigbeder J, Garay H, Bergeret A, Bénézet JC, Desauziers V. Correlation between artificial and natural weathering of hemp fibers reinforced polypropylene biocomposites. Polym Degrad Stab 2018;148:117–31. https://doi.org/10.1016/j.polymdegradstab.2018.01.002.

[22] Chang BP, Mohanty AK, Misra M. Studies on durability of sustainable biobased composites: a review. RSC Adv 2020;10:17955–99. https://doi.org/10.1039/c9ra09554c.

[23] Azwa ZN, Yousif BF, Manalo AC, Karunasena W. A review on the degradability of polymeric composites based on natural fibres. Mater Des 2013;47:424–42. https://doi.org/10.1016/j.matdes.2012.11.025.

[24] Sadeghifar H, Ragauskas A. Lignin as a UV Light blocker-a review. Polymers (Basel) 2020;12:1–10. https://doi.org/10.3390/POLYM12051134.

[25] Peng Y, Liu R, Cao J, Chen Y. Effects of UV weathering on surface properties of polypropylene composites reinforced with wood flour, lignin, and cellulose. Appl Surf Sci 2014;317:385–92. https://doi.org/10.1016/j.apsusc.2014.08.140.

[26] Stark NM, Matuana LM, Clemons CM. Effect of processing method on surface and

weathering characteristics of wood-flour/HDPE composites. J Appl Polym Sci 2004;93:1021–30. https://doi.org/10.1002/app.20529.

[27] Ratanawilai T, Taneerat K. Alternative polymeric matrices for wood-plastic composites: Effects on mechanical properties and resistance to natural weathering. Constr Build Mater 2018;172:349–57. https://doi.org/10.1016/j.conbuildmat.2018.03.266.

[28] Koffi A, Koffi D, Toubal L. Mechanical properties and drop-weight impact performance of injection-molded HDPE/birch fiber composites. Polym Test 2021;93:106956. https://doi.org/10.1016/j.polymertesting.2020.106956.

[29] Puech L, Ramakrishnan KR, Le Moigne N, Corn S, Slangen PR, Duc A Le, et al. Investigating the impact behaviour of short hemp fibres reinforced polypropylene biocomposites through high speed imaging and finite element modelling. Compos Part A Appl Sci Manuf 2018;109:428–39. https://doi.org/10.1016/j.compositesa.2018.03.013.

[30] Pillay S, Vaidya UK, Janowski GM. Effects of moisture and UV exposure on liquid molded carbon fabric reinforced nylon 6 composite laminates. Compos Sci Technol 2009;69:839–46. https://doi.org/10.1016/j.compscitech.2008.03.021.

[31] Roux C, Robertson J, Acid I, Acid D, Acid L. FIBERS | Types n.d.

[32] Sierra Beltran MG, Schlangen E. Wood fibre reinforced cement matrix: A micromechanical based approach. Key Eng Mater 2008;385–387:445–8. https://doi.org/10.4028/www.scientific.net/kem.385-387.445.

[33] Marchessault RH. Wood chemistry, fundamentals and applications. vol. 252. 1994. https://doi.org/10.1016/0008-6215(94)90030-2.

[34] Thygesen A, Madsen B, Bjerre AB, Lilholt H. Cellulosic fibers: Effect of processing on fiber bundle strength. J Nat Fibers 2011;8:161–75. https://doi.org/10.1080/15440478.2011.602236.

[35] Shahria S. Fabrication and Property Evaluation of Hemp–flax Fiber Reinforced Hybrid Composite. Chem Mater Eng 2019;7:17–23. https://doi.org/10.13189/cme.2019.070202.

[36] Komaki K, Kuroda T. Mechanical properties of FRP. J Soc Mater Sci Japan

1972;21:899–905. https://doi.org/10.2472/jsms.21.899.

[37] Pine Wood _ Properties, Price & Application _ Material Properties n.d.

[38] Bravo A, Toubal L, Koffi D, Erchiqui F. Damage characterization of bio and green polyethylene-birch composites under creep and cyclic testing with multivariable acoustic emissions. Materials (Basel) 2015;8:7322–41. https://doi.org/10.3390/ma8115382.

[39] Bravo A, Toubal L, Koffi D, Erchiqui F. Characterization of Tensile Damage for a Short Birch Fiber-reinforced Polyethylene Composite with Acoustic Emission. Int J Mater Sci 2013;3:79–89.

[40] Peng Y, Wang W, Cao J, Guo X. Effects of a layered double hydroxide (LDH) on the photostability of wood flour/polypropylene composites during UV weathering. RSC Adv 2015;5:41230–7. https://doi.org/10.1039/c5ra04999g.

[41] Horikawa Y, Hirano S, Mihashi A, Kobayashi Y, Zhai S, Sugiyama J. Prediction of Lignin Contents from Infrared Spectroscopy: Chemical Digestion and Lignin/Biomass Ratios of Cryptomeria japonica. Appl Biochem Biotechnol 2019;188:1066–76. https://doi.org/10.1007/s12010-019-02965-8.

[42] Badji C, Beigbeder J, Garay H, Bergeret A, Bénézet JC, Desauziers V. Exterior and under glass natural weathering of hemp fibers reinforced polypropylene biocomposites: Impact on mechanical, chemical, microstructural and visual aspect properties. vol. 148. Elsevier Ltd; 2018. https://doi.org/10.1016/j.polymdegradstab.2017.12.015.

[43] Samanta AK. Application of natural dyes to cotton and jute textiles: Science and technology and environmental issues. 2018. https://doi.org/10.1002/9781119407850.ch11.

[44] Del Río JC, Rencoret J, Gutiérrez A, Nieto L, Jiménez-Barbero J, Martínez ÁT. Structural characterization of guaiacyl-rich lignins in flax (Linum usitatissimum) fibers and shives. J Agric Food Chem 2011;59:11088–99. https://doi.org/10.1021/jf201222r.

[45] Rowell R, Pettersen R, Tshabalala M. Cell Wall Chemistry. 2012. https://doi.org/10.1201/b12487-5.

[46] Stark NM, Rowlands RE. Effects of wood fiber characteristics on mechanical properties of wood/polypropylene composites. Wood Fiber Sci 2003;35:167–74.

[47] Campos A, Marconcini JM, Martins-Franchetti SM, Mattoso LHC. The influence of UV-C irradiation on the properties of thermoplastic starch and polycaprolactone biocomposite with sisal bleached fibers. Polym Degrad Stab 2012;97:1948–55. https://doi.org/10.1016/j.polymdegradstab.2011.11.010.

Conflict of interest: Authors declare that they have no conflict of interest.

Human/Animal Rights: This article does not contain any studies with human or animal subjects performed by any of the authors.

Declaration of interests

☒The authors declare that they have no known competing financial interests or personal relationships that could have appeared to influence the work reported in this paper.

☐The authors declare the following financial interests/personal relationships which may be considered as potential competing interests:

Lotfi Toubal reports financial support was provided by Natural Sciences and Engineering Research Council of Canada (2460134).